Instability growth rates of crossing sea states

F. E. Laine-Pearson*
Department of Mathematics, University of Surrey, Guildford, Surrey GU2 7XH, United Kingdom
(Received 7 September 2009; revised manuscript received 16 February 2010; published 18 March 2010)

Crossing sea states can occur during adverse weather conditions. The instability of such wave trains has been suggested as a possible mechanism for the formation of rogue (freak or extreme) waves. One model for crossing sea states is weakly nonlinear and finite-amplitude short-crested waves (SCWs) on deep water. SCWs are the resonant interaction of two wave systems each with a different direction of propagation. Recently, it has been shown that the stability of these wave interactions is closely associated with the stability of the oblique nonresonant interaction between two waves. The long-wave instability of such waves is considered here; SCWs are used as a benchmark. By using a mismatch of amplitudes, it is demonstrated that instability growth rates of two crossing waves can be larger than those given by SCWs. This indicates that only considering true resonant interactions can underestimate the contribution from unstable crossing sea states to the possible formation of rogue waves.

DOI: 10.1103/PhysRevE.81.036316 PACS number(s): 47.35.−i, 92.10.Hm

I. INTRODUCTION

Rogue waves are spatially and temporally localized water surface excitations with extraordinarily large amplitude, exceeding the wave train height predicted by linear theory, and usually occur far out at sea [1–3]. According to Müller *et al.* [1], the largest wave observed in the Pacific was 34 m—this event occurred in the early 1900s, with the height obtained by lining up the wave crest with a line from the top of the foremast to the bridge. Nowadays, wave heights are calculated by less *ad hoc* methods. The most famous rogue wave of recent years is the "Draupner wave," which was confirmed by scientific evidence following measurements at the Draupner oil platform—wave records indicate a height of over 25 m [4].

There are a number of suggested mechanisms for the formation of these dangerous, and potentially life taking, waves [5,6]. Here, we shall concentrate on one in particular. Namely, for waves in deep water, a rogue wave may occur by natural, nonlinear processes from a random background of smaller waves. The nonlinear effects of a single modulated water wave train can be modeled by a nonlinear Schrödinger (NLS) Eq. [7,8]. The physical behavior of an unstable mode of such an NLS equation is governed by the Benjamin-Feir instability [9], which can lead to the formation of rogue waves [8,10–12].

A logical extension is to consider the interaction of two wavetrains. Crossing sea states occur when separate wave trains, propagating in different directions, meet. The combined interaction can be called a two-phase wave train. Interestingly, during the Draupner incident, the sea state consisted of two sea systems [4]. Indeed, renewed interest in sea state directionality has been seen in recent articles; for instance Donelan and Magnusson [13] considered the linear superposition of waves with different direction of propagation, whereas Osborne *et al.* [14] combined sea state directionality with the nonlinear, self-focusing mechanism of coupled NLS (CNLS) equations in $(1+1)$ dimensions, that is of (x,t).

More recently, the instability of two-phase wave trains has been highlighted by Onorato *et al.* [15] by using CNLS equations in $(2+1)$ dimensions, that is of (x,y,t), which was derived from the Zakharov formulation [16]. They showed the dynamics of the pair of weakly nonlinearly interacting water waves can be reduced to a $(1+1)$ CNLS system, much like Roskes' [17], when considering a stability analysis for perturbations along a single axis. By considering a basic plane wave solution of two CNLS equations, they demonstrated that a pair of carrier waves can have much larger modulational instability growth rates than a single carrier wave.

Following the work of Onorato *et al.* [15], Shukla *et al.* [18] extended the analysis to incorporate perturbations in two directions. They derived a nonlinear dispersion relation, which was numerically analyzed to obtain the regions, and the associated growth rates, of the modulational instability. In particular, the numerical analysis of the dynamical system revealed that a pair of water waves can, when nonlinear interactions are taken into account, give rise to behavior such as the formation of large-amplitude wave packets with amplitudes of more than triple the initial waves.

In this paper, a theory for the long-wave instability of short-crested waves (SCWs) will be reviewed. This review summarizes some of the work presented by Bridges and Laine-Pearson [19], which embeds SCWs within general two-wave interactions governed by generalized Hamiltonian partial differential equations (that is, multisymplectic systems). The advantage of this formulation is that it applies to the full water-wave problem. Hence, it includes everything that CNLS equations would get, and also includes other cases, including large amplitude waves. So this approach is more general than those used by Onorato *et al.* [15] and Shukla *et al.* [18].

In Bridges and Laine-Pearson [19], stability results are given for both transverse and longitudinal instabilities of SCWs. However, the growth rates of these instabilities were not investigated. The aim of this paper is to demonstrate that considering more general two-wave interactions can provide

*f.laine-pearson@surrey.ac.uk

leading order instability growth rates that are larger than those for SCWs (i.e., resonant interactions). This will be achieved by analyzing the water wave equations directly using multisymplectic theory [19], which will show a more general way to recover and extend the results of Onorato *et al.*

II. WEAKLY NONLINEAR TWO-WAVE INTERACTIONS FOR WATER WAVES

Our starting point is water waves on an inviscid, irrotational, infinite depth fluid of constant density. Let $(x,y) \in \mathbb{R}^2$ denote the horizontal coordinates and z the vertical coordinate. The fluid is bounded above by the surface $z=\eta(x,y,t)$. In the interior of the fluid, the velocity potential $\phi(x,y,z,t)$ satisfies Laplace's equation

$$\Delta\phi = \phi_{xx} + \phi_{yy} + \phi_{zz} = 0 \quad \text{for} \quad -\infty < z < \eta(x,y,z,t),$$

where subscripts denote partial differentiation, and is quiescent far from the surface

$$\nabla\phi \to 0 \quad \text{as} \quad z \to -\infty.$$

At the free surface, the functions (ϕ,η) satisfy the kinematic and dynamic boundary conditions

$$\left.\begin{aligned} \eta_t + \phi_x\eta_x + \phi_y\eta_y - \phi_z = 0 \\ \phi_t + \frac{1}{2}(\phi_x^2 + \phi_y^2 + \phi_z^2) + g\eta = 0 \end{aligned}\right\} \quad \text{at} \quad z = \eta(x,y,t),$$

where g is the gravitational constant.

At the linear level, a two-wave interaction solution of the above water wave equations is

$$\eta(x,y,t) = A_1 e^{i\theta_1} + A_2 e^{i\theta_2} + \text{c.c.},$$

$$\phi(x,y,z,t) = b_1 e^{\nu_1 z + i\theta_1} + b_2 e^{\nu_2 z + i\theta_2} + \text{c.c.},$$

for any complex numbers A_j and b_j, and where $\theta_j = k_j x + \ell_j y + \omega_j t$, $\nu_j = \sqrt{k_j^2 + \ell_j^2}$, for $j=1,2$, and "c.c." denotes complex conjugate. There is an arbitrary phase shift in each θ_j, which is suppressed. Additionally, at the linear level, $D(\omega_j,k_j,\ell_j)=0$ for $j=1,2$, where $D(\omega,k,\ell)$ is the dispersion function. For gravity waves, in infinite depth, $D(\omega,k,\ell)=\omega^2/\nu - g$.

The simplest nonlinear problem of pairwise interactions is to study the persistence of such a wave interaction in the nonlinear problem for small amplitude. For weakly nonlinear two-wave interactions for water waves, a leading-order expansion for the free-surface elevation and velocity potential is

$$\eta(x,y,t) = A_1 e^{i\theta_1} + A_2 e^{i\theta_2} + a_{21} + a_{22}e^{2i\theta_1} + a_{23}e^{2i\theta_2} + a_{24}e^{i(\theta_1+\theta_2)} + a_{25}e^{i(\theta_1-\theta_2)} + \text{c.c.} + \cdots, \quad (1a)$$

$$\phi(x,y,z,t) = b_1 e^{\nu_1 z + i\theta_1} + b_2 e^{\nu_2 z + i\theta_2} + b_{22}e^{2(\nu_1 z + i\theta_1)} + b_{23}e^{2(\nu_2 z + i\theta_2)} + b_{24}e^{\chi_+ z + i(\theta_1+\theta_2)} + b_{25}e^{\chi_- z + i(\theta_1-\theta_2)} + \text{c.c.} + \cdots, \quad (1b)$$

with complex numbers a_{mn} and b_{mn}, and where

$$\chi_+^2 = \nu_1^2 + \nu_2^2 + 2\nu_1\nu_2\cos\gamma, \quad \chi_-^2 = \nu_1^2 + \nu_2^2 - 2\nu_1\nu_2\cos\gamma,$$

and where the angle γ is the angle between the wave vectors (k_1,ℓ_1) and (k_2,ℓ_2), defined as $\cos\gamma = (k_1k_2 + \ell_1\ell_2)/(\nu_1\nu_2)$.

From the weakly nonlinear theory described in [19], a set of amplitude equations is found,

$$[(\omega_1^2/\nu_1 - g) - 4\nu_1\omega_1^2|A_1|^2 + \Upsilon|A_2|^2 + \cdots]A_1 = 0,$$

$$[(\omega_2^2/\nu_2 - g) + \Upsilon|A_1|^2 - 4\nu_2\omega_2^2|A_2|^2 + \cdots]A_2 = 0,$$

where

$$\Upsilon = \frac{\omega_1\omega_2}{g}(\omega_1+\omega_2)^2 K_+ \sin^2(\gamma/2) - \frac{\omega_1\omega_2}{g}(\omega_1 - \omega_2)^2 K_- \cos^2(\gamma/2) - 8\omega_1\omega_2(\nu_1+\nu_2)\cos\gamma + \frac{2}{g}\omega_1^2\omega_2^2(3 + \cos^2\gamma),$$

$$K_+ = \frac{16\omega_1\omega_2\sin^2(\gamma/2)}{g\chi_+ - (\omega_1+\omega_2)^2}, \quad K_- = -\frac{16\omega_1\omega_2\cos^2(\gamma/2)}{g\chi_- - (\omega_1-\omega_2)^2}.$$

The above set is the weakly nonlinear analog of the linear dispersion relation $\omega_j^2/\nu_j = g$. Note that if $|A_2|=0$ and $|A_1| \neq 0$, or vice versa, the weakly nonlinear dispersion relation for a plane monochromatic wave is recovered. When $|A_1||A_2| \neq 0$, the nonlinear frequency change as a function of amplitude for the (generically) quasiperiodic two-wave interaction is obtained.

Consider a linear perturbation around the equilibrium (basic) state (1) with the wave vector (α,β) and the frequency Ω; α and β are real and $\Omega \in \mathbb{C}$. Substitution of the perturbed equilibrium state into the water wave equations, and linearizing about the basic state, then expanding the resulting eigenvalue problem for the stability exponent Ω in a Taylor series in α and β with the restriction $|\alpha|^2 + |\beta|^2 \ll 1$, will result in a solvability condition that will reveal the leading-order behavior of the stability exponent Ω. It is noted that, although attention is restricted to long-wave instabilities (where $|\alpha|^2 + |\beta|^2 \ll 1$), this hypothesis does not put any restriction on the amplitudes of the basic state, it restricts only the class of perturbation. Further details on the perturbation process are given in [19]. It turns out that there is a nontrivial solution of the linear stability problem if and only if

$$\Delta(\Omega,\alpha,\beta) := g_4\Omega^4 + g_3\Omega^3 + g_2\Omega^2 + g_1\Omega + g_0 = 0. \quad (2)$$

The g_j for SCWs ($|A_1|=|A_2|$) are given in [19]. However, the g_j can be calculated for the more general case where $|A_2| \neq |A_1|$. These are given in the Appendix.

The following definition of instability is of relevance: *If for some* $(\alpha,\beta) \in \mathbb{R}^2$ there exists an $\Omega \in \mathbb{C}$ such that $\Delta(\Omega,\alpha,\beta)=0$ and $\Im(\Omega) \neq 0$ the basic state is linearly unstable. Solving the quartic Eq. (2) will give the leading-order behavior of the roots Ω.

Here, the simplest type of nonresonant interaction is of interest. Namely, mismatched amplitudes: $|A_2| = \mu|A_1| = \mu|A|$ where $\mu \in \mathbb{R}^+$ and $A \in \mathbb{C}$. Therefore, for a straightforward comparison with SCWs, set $k_2=k_1=k$, $\ell_2=-\ell_1=-\ell$, $\omega_2=\omega_1=q\omega$ where $q=\pm 1$. This will result in $\nu_1=\nu_2=\nu$ as well as

$|\Lambda|=a^2-b^2$ with $a=-4\nu\omega^2=-4g\nu^2$ and $b=\Upsilon$ evaluated at the SCW limit (as the amplitudes do not appear explicitly in Υ). Additionally, it is prescribed that $\nu\neq 0$ and $a\neq\pm b$ (so $|\Lambda|\neq 0$). These assumptions are made in the theory [19] to prevent zero divisors.

The amplitudes are now $|A_1|=|A|$ and $|A_2|=\mu|A|$. Therefore, $\mu=|A_2|/|A_1|$, the ratio of amplitudes. Resonant interactions require $\mu=1$ and non- resonant interactions require $\mu\neq 1$.

Before determining the growth rate, first introduce the natural normalization that follows. Let $A=A'/\nu$, and

$$\alpha=\alpha'\nu,\quad \beta=\beta'\nu,\quad k=k'\nu,\quad \ell=\ell'\nu,\quad \Omega=\Omega'\omega.$$

Also let $k=\nu\cos\theta$ and $\ell=\nu\sin\theta$, where θ is the angle between the wave directions and the $\ell=0$ axis. With the exception of numerical factors, Eq. (2) now only contains the angle θ, the scaling μ, the known wave numbers α' and β', the wave amplitude A' and the unknown frequency Ω'.

III. INSTABILITY GROWTH RATES FOR RESONANT INTERACTIONS

The instability growth rates for resonant interactions ($\mu=1$) are given in the literature by Onorato *et al.* [15] and Shukla *et al.* [18]. These known results will be referred to so that the method used in this paper can be validated.

To determine the growth rates, Ω must be found. The leading order form of Ω is determined from the quartic Eq. (2). Taking the imaginary part will give the growth rates. The $\Im(\Omega)$ here is equivalent to $\Im(2\Omega)$ of [15,18]. Therefore, for ease of comparison, the growth rate will be expressed as $\Gamma=\Im(\Omega'/2)$, which uses the natural normalization introduced earlier. Additionally, to correspond with the analyses of [15,18], set $A'=0.1$ (so that $A=0.1/\nu$) and $q=-1$.

For longitudinal stability ($\beta=0$), the results will be validated with those of Onorato *et al.* [15]. The approach taken by [15] resulted in a formula for the instability growth rate where the wave number of the perturbation α appears up to second order. However, the theory [19] used here only considers leading-order terms, which are first order. As a consequence, the benchmarking of the method used in this paper against [15] will show the regions of validity for the linearization. Graphical output from both methods will be used for comparison. Figure 1 shows a selection of growth graphs for various θ when $\beta=0$. These graphs will now be explained in more detail.

The θ angles fixed in Fig. 1 have been chosen to show representative growth rates for different regions of stability. Calculations of the stability regions are given in [19]; the angle 'θ' there corresponds to "$\theta-90°$" here. There are four distinct θ stability regions. Three are unstable and one is stable.

In the regions $0°<\theta<27°$ and $68°<\theta<90°$ there is one (complex conjugate) pair of unstable eigenvalues and so only one instability growth rate exists. Figure 1(a) is an example of the former, whereas Fig. 1(c) is an example of the latter. In the interval $27°<\theta<35°$ there are two pairs of unstable eigenvalues. This means there will be two instability growth rates, one for each pair of unstable eigenvalues. Figure 1(b) illustrates two such leading-order instability growth rate lines. The fourth interval is $35°<\theta<68°$, where all roots are stable. Therefore no instability growth rate exists.

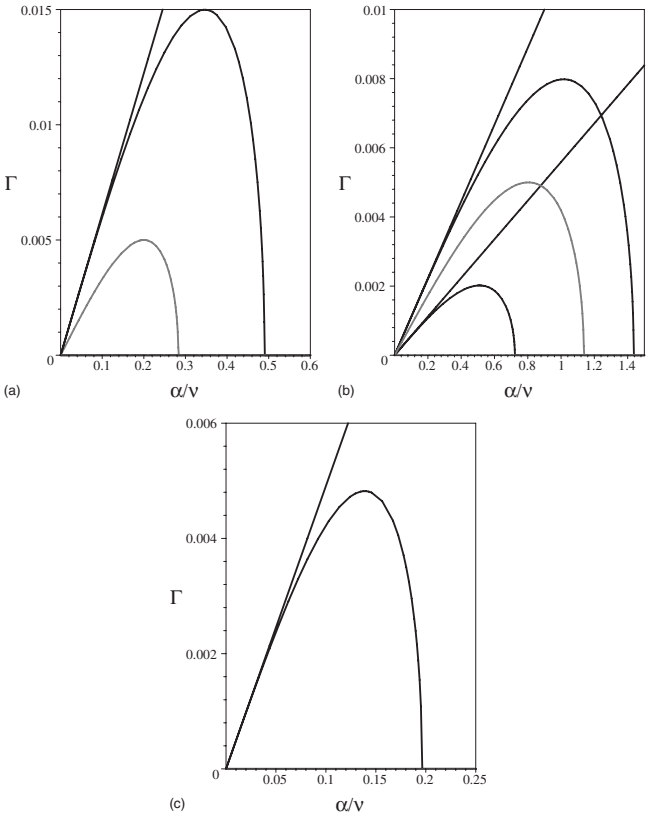

FIG. 1. Nondimensional growth rates Γ for longitudinal perturbation ($\beta=0$) of a single carrier wave (gray curves) and two carrier waves (black curves), both from NLS systems, as well as SCWs on deep water (black straight lines). The straight lines are leading-order growth rates that represent the linearization. The curves include second-order contributions for normalized wave number of the perturbation $\alpha'=\alpha/\nu$ appearing in higher-order calculations of Onorato *et al.* [15]. The fixed angles are (a) $\theta=1°$, (b) $\theta=34°$, and (c) $\theta=89°$.

Using the equation given for the growth rate in Onorato *et al.* [15], the curves for single carrier waves and two carrier waves have been reproduced. Second-order terms create the humped appearance. The straight lines are from solving Eq. (2) to leading order and so represent the linearization. There is good correspondence for sufficiently small values of the wave number perturbation (that is, whenever $\alpha'=\alpha/\nu$ is small enough). In particular, the linearization is a fair representation of the higher-order calculations whenever $\alpha'<0.1$, $\alpha'<0.2$, $\alpha'<0.05$, for Figs. 1(a)–1(c), respectively.

For transverse instability (β is small but outside a neighborhood of $\beta=0$) the results can be compared with Shukla *et al.* [18]. The approach taken by [18] resulted in a nonlinear dispersion relation that needed to be solved numerically for the growth rates. The wave numbers of perturbation $\alpha'=\alpha/\nu$ and $\beta'=\beta/\nu$ appear up to second order for the growth rates. The theory [19] used here only considers the linearization, so only leading-order terms in α' and β' appear. As a consequence, only first-order phenomena can be compared. However, this will give the regions of validity for the lin-

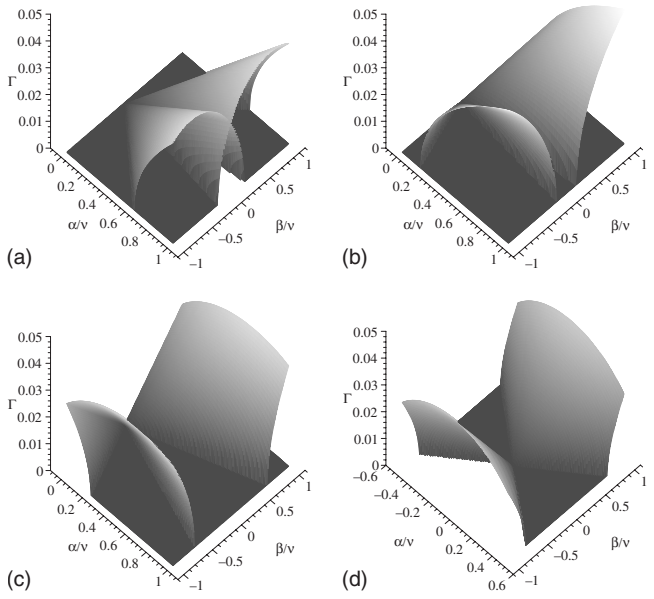

FIG. 2. Three-dimensional view of nondimensional growth rates Γ for transverse perturbation ($\beta \neq 0$) of SCWs on deep water. The surfaces are calculated using leading order terms only. The fixed angles are: (a) $\theta=\pi/8$, (b) $\theta=\pi/4$, (c) $\theta=3\pi/8$, and (d) $\theta=\pi/2$.

erization. Figures 2 and 3 illustrate the growth rate surfaces that must be compared with Shukla *et al.* [18] who plotted similar surfaces using their method that includes higher-order calculations.

The leading-order behavior of the growth rate when $\beta \neq 0$ is shown in Fig. 2. The corresponding bird's eye views are shown in Fig. 3. The angle θ is fixed in each instance. The choice of angle for Figs. (a), (b), and (d) comes from Shukla *et al.* [18]. In Bridges and Laine-Pearson [19], the different types of instability are related to the angle θ; the angle "θ" there corresponds to "$\theta-90°$" here. Their Fig. 7 (three diagrams) illustrates these types for (α,β) sufficiently small. They directly correspond to Figs. 3(a)–3(c). To make a straightforward comparison, Fig. 4 zooms into the appropriate regions of Fig. 3. The gray coloring represents specific types of instability. Light gray areas represent one unstable mode. Dark gray areas represent two unstable modes. Figure 4(a) is indicative of instability for $0° < \theta < 35.27°$, which produces two unstable areas; in the lower triangle (dark gray) there are two unstable modes and in the central region (light gray) there is one unstable mode. Figure 4(b) is indicative of instability for $35.27° < \theta < 54.74°$, which produces one central unstable region (light gray) containing one unstable mode. Figure 4(c) is indicative of instability for $54.74° < \theta < 90°$, which produces two unstable areas; in the upper triangle (dark gray) there are two unstable modes and in the central region (light gray) there is one unstable mode. The limit $\theta \to 90°$ corresponds to the standing wave limit. The strongest region of instability is predominantly in the y direction, which is consistent with the modulation instability of pure standing waves. Figure 4(d) is indicative of instability for the standing wave limit; the single upper triangle (dark gray) contains two unstable modes.

Focusing specifically on the growth rates, Figs. 3(a), 3(b), and 3(d) have been plotted to show the growth rate Γ restricted to the interval shown in [18]. Specifically, $\Gamma \leq 0.01$ for Figs. 3(a) and 3(d) and $\Gamma \leq 0.005$ for Fig. 3(b). [Incidentally, $\Gamma \leq 0.005$ for Fig. 3(c) as well.] Figs. 3(a), 3(b), and 3(d) correspond to Shukla *et al.*'s Figs. 1–3, respectively. On inspection, these figures are comparative to leading order. However, the higher order terms that Shukla *et al.* include produce additional distinct humped areas for $\theta=\pi/8$ and $\theta=\pi/2$. Referring to Shukla *et al.* [18], these minor humps appear for $\theta=\pi/8$ when $\alpha' < 0.5$ and $|\beta'| > 0.9$ as well as when $\alpha' > 0.7$ and $0.1 < |\beta'| < 0.3$. Other humps emanate in two symmetric, slightly curved v shapes for $\theta=\pi/2$ when $|\alpha'| \leq 0.5$ and $|\beta'| < 0.2$. When (α',β') are sufficiently small, these second-order phenomena become irrelevant for $\theta=\pi/8$ and only give growth rates comparable to leading-order humps for $\theta=\pi/2$. As the data sets used to produce the plots in Shukla *et al.* are not explicitly given in their paper, accurate determination of the regions of validity for the linearization is not possible. However, an estimate can be given by referring to Shukla *et al.*'s color interval charts for each fixed θ plot. This is done by focusing on a square-shaped area of (α',β') centered on the origin and enlarging the area until the approximate maximum growth rate of Shukla *et al.* becomes noticeably different to the exact maximum found in the corresponding plot in Fig. 3. For Figs. 3(a) and 3(b) there is reasonable correspondence for $\alpha' < 0.1$ and $|\beta'| < 0.1$. For Fig. 3(d) there is reasonable correspondence for $|\alpha'| < 0.1$ and $|\beta'| < 0.1$. Both sets of intervals result in $(\alpha')^2$ and $(\beta')^2$ each of order 10^{-2}, which is very small. Therefore these intervals will be taken as the regions of validity for the linearization.

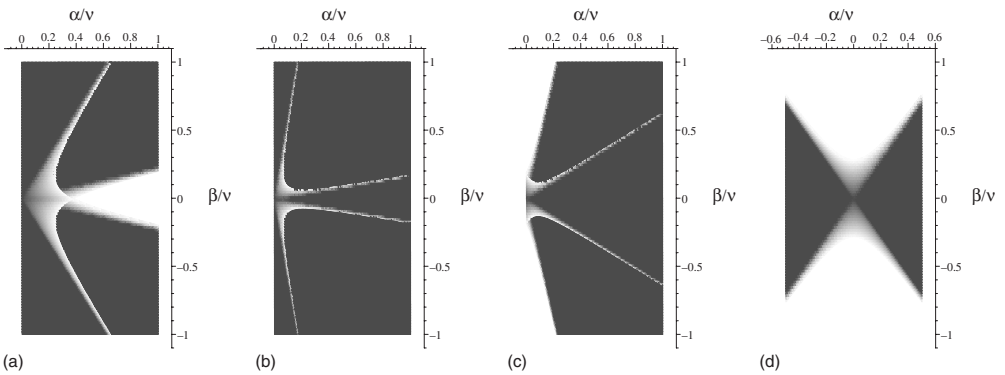

FIG. 3. Bird's eye view of nondimensional growth rates Γ for transverse perturbation ($\beta \neq 0$) of SCWs on deep water. The surfaces are calculated using leading order terms only. The fixed angles are (a) $\theta=\pi/8$, (b) $\theta=\pi/4$, (c) $\theta=3\pi/8$, and (d) $\theta=\pi/2$.

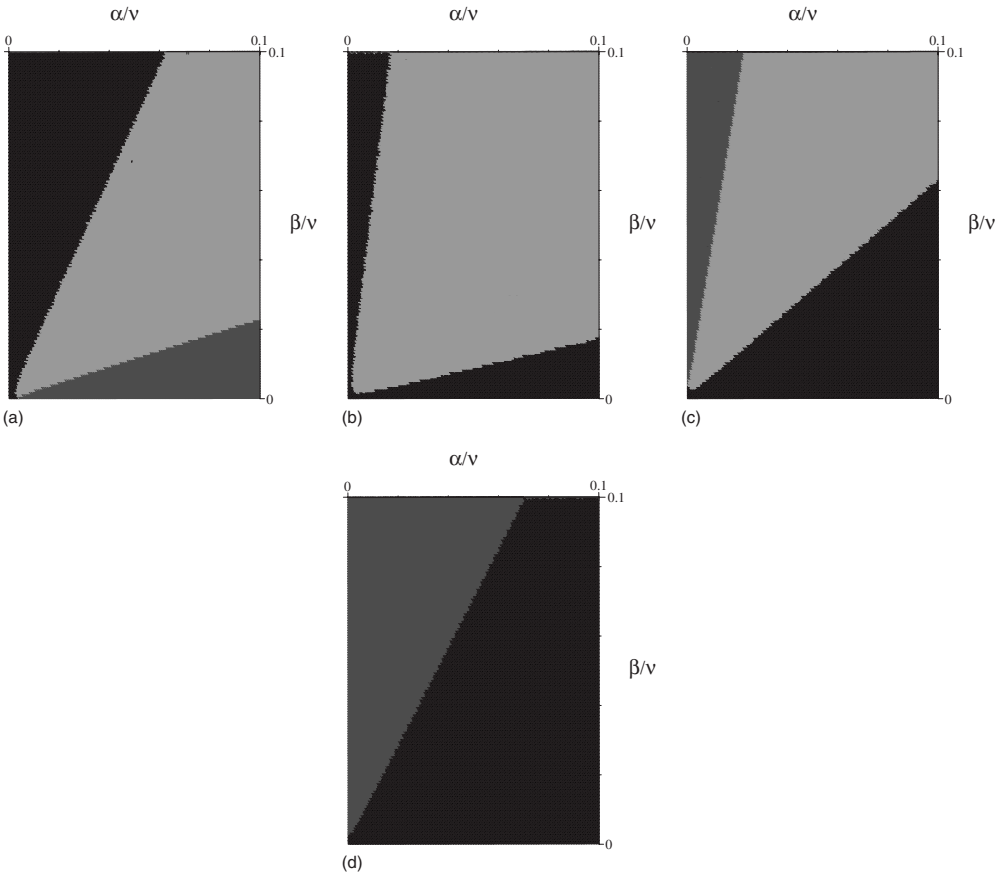

FIG. 4. Bird's eye view of nondimensional growth rates Γ for transverse perturbation ($\beta \neq 0$) of SCWs on deep water for small $\alpha' = \alpha/\nu$ and $\beta' = \beta/\nu$. The surfaces are calculated using leading order terms only. The fixed angles are: (a) $\theta = \pi/8$, (b) $\theta = \pi/4$, (c) $\theta = 3\pi/8$, and (d) $\theta = \pi/2$. The different colored areas indicate specific types of instability. Light gray areas represent one unstable mode. Dark gray areas represent two unstable modes.

IV. INSTABILITY GROWTH RATES FOR NON-RESONANT INTERACTIONS

The regions of validity for the linearization have been determined in the previous section. The next step is to analyze the growth rates for non-resonant interactions ($\mu \neq 1$) within these regions. Therefore, attention is restricted to sufficiently small $\alpha' = \alpha/\nu$ and $\beta' = \beta/\nu$. This is so a fair comparison is made.

The difference in growth rates between resonant interactions ($\mu = 1$) and nonresonant interactions ($\mu \neq 1$) are best displayed graphically. Figure 5 shows the growth rates for various μ for longitudinal stability ($\beta = 0$). The interval for the normalized wave number of the perturbation α' was chosen from considering Fig. 1 where the linearization is a fair representation of higher-order calculations.

The black surfaces in Fig. 5 extend the growth rate lines when $\mu = 1$ each to a plane for comparison with surfaces drawn when $\mu \neq 1$. For $0 < \mu < 1$ the growth rate is smaller when there is only one pair of unstable eigenvalues. However, when $\mu > 1$ the growth rate increases as μ increases. When there are two pairs of unstable eigenvalues, the lower surface (dark gray) doesn't follow this pattern. However the higher surface (light gray), which has the greater Γ values, does.

Growth rates for transverse stability ($\beta \neq 0$) can be visualized in $(\alpha', \beta', \Gamma)$-space for fixed θ and various μ. Illustrative examples are shown in Fig. 6. The intervals for the normalized wave number of the perturbations (α', β') were chosen from considering Fig. 3 where the linearization is a fair representation of higher-order calculations. The growth rate surfaces of Fig. 6 are qualitatively similar to those shown in Fig. 2. Therefore, choosing $\mu \neq 1$ results in quantitative changes that are scaled in a self-similar way to the resonant case.

To appreciate the differences for growth rate surfaces between the cases $\mu = 1$ and $\mu \neq 1$, first consider Figs. 6(a) and 6(b). Comparing with Figs. 2(a) and 2(b), respectively, it is clear that the right-hand wing surface does not vary as μ varies. This is because the scaling μ doesn't appear in the linearization for a pair of roots Ω. The other pair of roots does contain the scaling μ and corresponds to the left-hand wing surface. Therefore, when $0 < \mu < 1$, the left-hand wing shrinks, neatly nested inside the $\mu = 1$ case. When $\mu > 1$, the left-hand wing enlarges so that the $\mu = 1$ case neatly fits inside it.

Now consider Figs. 6(c) and 6(d). These figures have been rotated 90° counterclockwise around the Γ axis compared with the orientation of Figs. 6(a), 6(b), and 2. This has been done to clearly show the changes to the growth rate surfaces. Figures 6(c) and 6(d) behave similarly to Figs. 6(a) and 6(b). Namely, one surface stays fixed in shape whereas the other varies as μ is varied. [This is not so noticeable for Fig. 6(d) as the two surfaces for the $\mu = 1$ case are so close together that they appear to be touching.] Furthermore, $0 < \mu < 1$ influences one surface to shrink and $\mu > 1$ influences the same surface to enlarge. The only difference in behavior between Fig. 6(c) and Figs. 6(a) and 6(b) is that, for $\mu \neq 1$, the two surfaces (each from different Ω pairs) now can intersect. This intersecting behavior is not seen for Fig. 6(d).

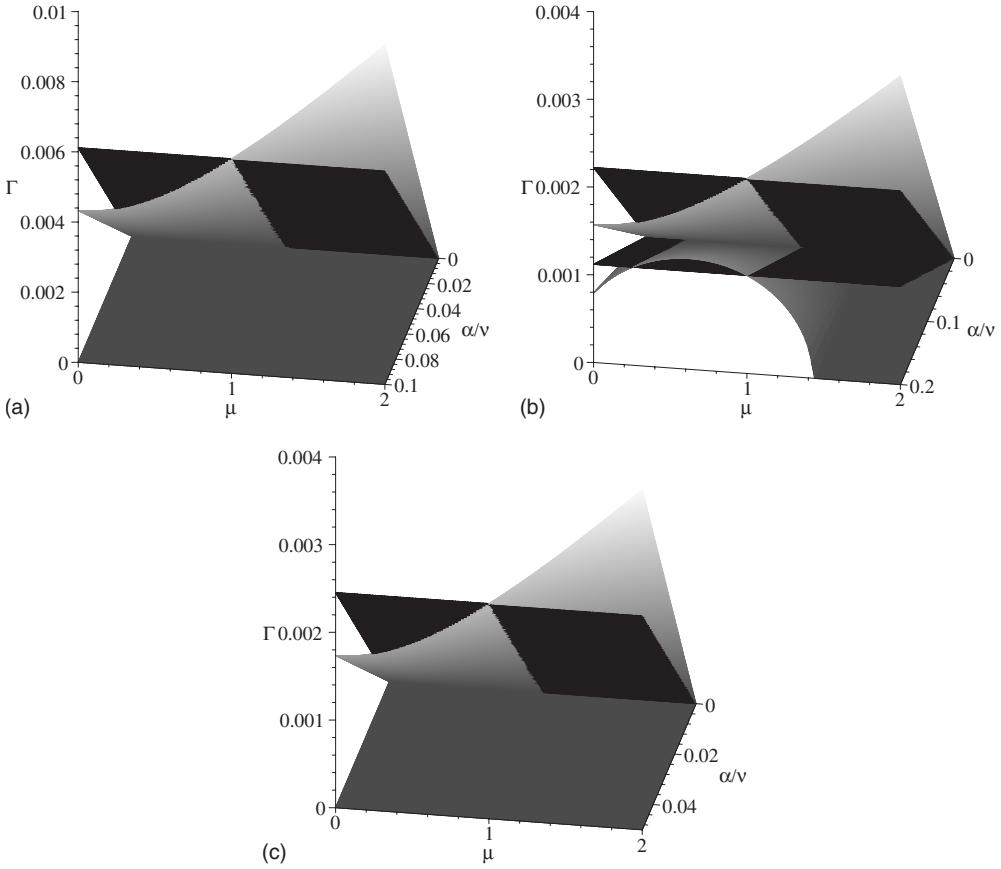

FIG. 5. Leading-order nondimensional growth rates Γ for longitudinal perturbations ($\beta=0$) of weakly nonlinear water waves. The fixed angles are: (a) $\theta=1°$, (b) $\theta=34°$, and (c) $\theta=89°$. The black surfaces extend the lines when $\mu=1$ each to a plane for comparison. The pale and dark gray surfaces each represent the growth rate of a pair of unstable eigenvalues. See text for details.

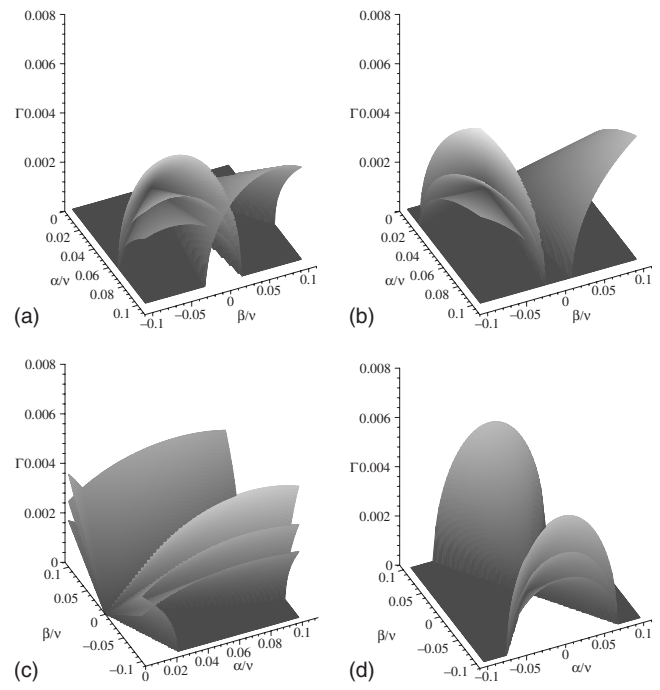

FIG. 6. Leading-order nondimensional growth rates Γ for transverse perturbations ($\beta\neq 0$) of weakly nonlinear water waves for various values of μ. The fixed angles are: (a) $\theta=\pi/8$, (b) $\theta=\pi/4$, (c) $\theta=3\pi/8$, and (d) $\theta=\pi/2$. The upper wing is for $\mu=2$. The lower wing is for $\mu=1/2$. The central wing is for the resonant case ($\mu=1$).

In conclusion, the size of the growth rate is dependent on the magnitude of μ. As $\mu=|A_2|/|A_1|$, this implies the growth rate is influenced by the ratio of the amplitudes. When $\mu>1$ ($|A_2|>|A_1|$), the largest growth rate for specific (α',β') can be greater than the corresponding growth rate for the resonant case. This indicates that non-resonant interactions can have noticeably larger growth rates than resonant interactions. Such occurrences are a direct result of one wave having a larger amplitude than the other.

V. SUMMARY

A model for weakly nonlinear and finite-amplitude waves on deep water was presented. This model was used to study the interaction of two-wave systems propagating in different wave directions, similar in nature to crossing sea states. Results show that leading-order growth rates for more general two-wave interactions can be larger than those for SCWs. Although the results are only leading-order, they do suggest that two-wave systems are potentially more volatile than previously indicated. It is speculated that this increased instability of colliding water waves may further encourage the production of rogue waves in deep water.

ACKNOWLEDGMENTS

The author thanks Prof. Thomas J. Bridges for consultation and the Department of Mathematics, at the University of Surrey, for its hospitality.

APPENDIX

The g_j are calculated for the simplest type of nonresonant interactions:

$$g_4 = \frac{D_w^4}{|\Lambda|} - a\frac{D_{\omega\omega}D_\omega^2}{|\Lambda|}(1+\mu)|A|^2 + \mu D_{\omega\omega}^2|A|^4 + \cdots,$$

$$g_3 = 2q\left[2\alpha\frac{D_\omega^3 D_k}{|\Lambda|} - a\frac{D_\omega}{|\Lambda|}G_{32}|A|^2 + 2\alpha\mu D_{\omega\omega}D_{\omega k}|A|^4\right] + \cdots,$$

$$g_2 = 2\frac{D_\omega^2}{|\Lambda|}(3\alpha^2 D_k^2 - \beta^2 D_\ell^2) - \frac{a}{|\Lambda|}G_{22}|A|^2 + 2\mu G_{24}|A|^4 + \cdots,$$

$$g_1 = \frac{4q}{|\Lambda|}\alpha D_\omega D_k G_{10} - \frac{2qa}{|\Lambda|}G_{12}|A|^2 + 4q\alpha\mu G_{14}|A|^4 + \cdots,$$

$$g_0 = \frac{1}{|\Lambda|}G_{00} - \frac{a}{|\Lambda|}G_{02}|A|^2 + \mu G_{04}|A|^4\cdots,$$

where

$$G_{32} = \alpha(\mu+1)(D_\omega D_{\omega k} + D_k D_{\omega\omega}) + \beta(\mu-1)(D_\ell D_{\omega\omega} + D_{\omega\ell}D_\omega),$$

$$G_{22} = \alpha^2(1+\mu)F_{20} + \alpha\beta(1-\mu)F_{21} + (1+\mu)\beta^2 F_{22},$$

$$G_{24} = \alpha^2(D_{\omega\omega}D_{kk} + 2D_{\omega k}^2) + \beta^2(D_{\omega\omega}D_{\ell\ell} - 2D_{\omega\ell}^2),$$

$$G_{10} = (\alpha D_k - \beta D_\ell)(\alpha D_k + \beta D_\ell),$$

$$G_{12} = \alpha\beta^2(1+\mu)F_{10} + \alpha^2\beta(1-\mu)F_{11} + \alpha^3(1+\mu)F_{12} + \beta^3(1-\mu)F_{13},$$

$$G_{14} = \beta^2(D_{\omega k}D_{\ell\ell} - 2D_{\omega\ell}D_{k\ell}) + \alpha^2 D_{\omega k}D_{kk},$$

$$G_{00} = (\alpha D_k - \beta D_\ell)^2(\alpha D_k + \beta D_\ell)^2,$$

$$G_{02} = \alpha^4 F_{00} + \beta^4 F_{01} + \alpha\beta^3 F_{02} + \alpha^2\beta^2 F_{03} + \alpha^3\beta F_{04},$$

$$G_{04} = (\beta^2 D_{\ell\ell} + 2\alpha\beta D_{k\ell} + \alpha^2 D_{kk})(\beta^2 D_{\ell\ell} - 2\alpha\beta D_{k\ell} + \alpha^2 D_{kk}),$$

with

$$F_{20} = 4D_\omega D_k D_{\omega k} + D_\omega^2 D_{kk} + D_{\omega\omega}D_k^2,$$

$$F_{21} = -2D_{\omega\omega}D_k D_\ell + 4D_\omega D_k D_{\omega\ell} + 2D_\omega^2 D_{k\ell} - 4D_{\omega k}D_\omega D_\ell,$$

$$F_{22} = -4D_\omega D_\ell D_{\omega\ell} + D_{\omega\omega}D_\ell^2 + D_\omega^2 D_{\ell\ell},$$

$$F_{10} = D_{\ell\ell}D_\omega D_k + D_\ell^2 D_{\omega k} - 2D_\ell(D_{k\ell}D_w + D_k D_{\omega\ell}),$$

$$F_{11} = -D_{kk}D_\omega D_\ell + D_k^2 D_{\omega\ell} - 2D_k(D_{k\ell}D_\omega + D_\ell D_{\omega k}),$$

$$F_{12} = D_k D_{\omega k} + D_\omega D_{kk},$$

$$F_{13} = D_{\ell\ell}D_\omega + D_\ell D_{\omega\ell},$$

$$F_{00} = (1+\mu)D_k^2 D_{kk},$$

$$F_{01} = (1+\mu)D_\ell^2 D_{\ell\ell},$$

$$F_{02} = (\mu-1)(2D_{\ell\ell}D_k D_\ell - 2D_\ell^2 D_{k\ell}),$$

$$F_{03} = (1+\mu)(D_\ell^2 D_{kk} + D_k^2 D_{\ell\ell} - 4D_k D_\ell D_{k\ell}),$$

$$F_{04} = (\mu-1)(2D_k D_\ell D_{kk} - 2D_k^2 D_{k\ell}).$$

Here, the subscripts on the D denote partial differentiation. The main text gives details of the parameters. It is noted there is a misprint for g_1 in [19] when $\mu=1$, which has been corrected here.

[1] P. Müller *et al.*, Oceanography **18**, 66 (2005).
[2] P. A. E. M. Janssen, *Proceedings of the Hawaiian Winter Workshop*, edited by P. Müller and D. Henderson (SOEST Publications, Honolulu, 2005).
[3] P. C. Lui and K. R. MacHutchon, *Proceedings of OMAE2006* (ASME, New York, 2006).
[4] S. Haver, *Proceedings of the Hawaiian Winter Workshop*, edited by P. Müller and D. Henderson (SOEST Publications, Honolulu, 2005).
[5] K. Dysthe, *Proceedings of Rogue Waves 2000*, edited by M. Olagnon and G. Athanassoulis (Ifremer, France, 2002).
[6] B. S. White and B. Fornberg, J. Fluid Mech. **355**, 113 (1998).
[7] C. Sulem and P.-L. Sulem, *The Nonlinear Schrodinger Equation: Self-focusing and Wave Collapse* (Springer, New York, 1999).
[8] A. R. Osborne *et al.*, Phys. Lett. A **275**, 386 (2000).
[9] T. B. Benjamin and J. E. Feir, J. Fluid Mech. **27**, 417 (1967).
[10] A. Calini and C. M. Schober, Phys. Lett. A **298**, 335 (2002).
[11] V. P. Ruban, Phys. Rev. E **74**, 036305 (2006).
[12] V. P. Ruban, Phys. Rev. Lett. **99**, 044502 (2007).
[13] M. A. Donelan and A. K. Magnusson, *Proceedings of the Hawaiian Winter Workshop*, edited by P. Müller and D. Henderson (SOEST Publications, Honolulu, 2005).
[14] A. R. Osborne *et al.*, *Proceedings of the Hawaiian Winter Workshop*, edited by P. Müller and D. Henderson (SOEST Publications, Honolulu, 2005).
[15] M. Onorato, A. R. Osborne, and M. Serio, Phys. Rev. Lett. **96**, 014503 (2006).
[16] V. E. Zakharov, Prikl. Mekh. Tekh. Fiz. **9**, 86 (1968) [J. Appl. Mech. Tech. Phys. **9**, 190 (1968)].
[17] G. J. Roskes, Stud. Appl. Math. **55**, 231 (1976).
[18] P. K. Shukla, I. Kourakis, B. Eliasson, M. Marklund, and L. Stenflo, Phys. Rev. Lett. **97**, 094501 (2006).
[19] T. J. Bridges and F. E. Laine-Pearson, J. Fluid Mech. **543**, 147 (2005).